

Article

# Airflow Characteristics Downwind a Naturally Ventilated Pig Building with a Roofed Outdoor Exercise Yard and Implications on Pollutant Distribution

Qianying Yi <sup>1,\*</sup>, David Janke <sup>1</sup>, Lars Thormann <sup>1</sup>, Guoqiang Zhang <sup>2</sup>, Barbara Amon <sup>3,4</sup>,  
Sabrina Hempel <sup>1</sup>, Štěpán Nosek <sup>5</sup>, Eberhard Hartung <sup>6</sup> and Thomas Amon <sup>1,7</sup>

<sup>1</sup> Department of Engineering for Livestock Management, Leibniz Institute for Agricultural Engineering and Bioeconomy (ATB), Max-Eyth-Allee 100, 14469 Potsdam, Germany; djanke@atb-potsdam.de (D.J.); LThormann@atb-potsdam.de (L.T.); shempel@atb-potsdam.de (S.H.); tamon@atb-potsdam.de (T.A.)

<sup>2</sup> Department of Engineering, Aarhus University, Inge Lehmanns Gade 10, 8000 Aarhus C, Denmark; guoqiang.zhang@eng.au.dk

<sup>3</sup> Department of Technology Assessment and Substance Cycles, Leibniz Institute for Agricultural Engineering and Bioeconomy (ATB), Max-Eyth-Allee 100, 14469 Potsdam, Germany; bamon@atb-potsdam.de

<sup>4</sup> Faculty of Civil Engineering, Architecture and Environmental Engineering, University of Zielona Góra, Licealna 9/9, 65-417 Zielona Góra, Poland

<sup>5</sup> Institute of Thermomechanics AS CR, v.v.i., Dolejškova 1402/5, 18200 Prague, Czech Republic; nosek@it.cas.cz

<sup>6</sup> Institute of Agricultural Process Engineering, Christian-Albrechts-University of Kiel (CAU), Max-Eyth-Straße 6, 24118 Kiel, Germany; ehartung@ilv.uni-kiel.de

<sup>7</sup> Institute of Animal Hygiene and Environmental Health, Department of Veterinary Medicine, Free University Berlin, Robert-von-Ostertag-Str. 7–13, 14163 Berlin, Germany

\* Correspondence: QYi@atb-potsdam.de

Received: 11 June 2020; Accepted: 15 July 2020; Published: 17 July 2020



**Abstract:** The application of naturally ventilated pig buildings (NVPBs) with outdoor exercise yards is on the rise mainly due to animal welfare considerations, while the issue of emissions from the buildings to the surrounding environment is important. Since air pollutants are mainly transported by airflow, the knowledge on the airflow characteristics downwind the building is required. The objective of this research was to investigate airflow properties downwind of a NVPB with a roofed outdoor exercise yard for roof slopes of 5°, 15°, and 25°. Air velocities downwind a 1:50 scaled NVPB model were measured using a Laser Doppler Anemometer in a large boundary layer wind tunnel. A region with reduced mean air velocities was found along the downwind side of the building with a distance up to 0.5 m (i.e., 3.8 times building height), in which the emission concentration might be high. Additional air pollutant treatment technologies applied in this region might contribute to emission mitigation effectively. Furthermore, a wake zone with air recirculation was observed in this area. A smaller roof slope (i.e., 5° slope) resulted in a higher and shorter wake zone and thus a shorter air pollutant dispersion distance.

**Keywords:** emission; turbulence; roof slope; scaled model; wind tunnel; dispersion

## 1. Introduction

Natural ventilation systems have the advantages of low capital investment, energy saving [1], and absence of noise [2] compared with mechanical ventilation systems. Thus, they are widely implemented in livestock buildings. Naturally ventilated pig production systems equipped with outdoor exercise yards are receiving increasing interest in Europe, the United States,

and South Africa [3,4]. This housing system provides pigs larger living areas, enables the separation of lying and excretion areas, and allows pigs to exhibit natural behaviours [5]. It provides pigs access to an outdoor exercise area, enables pigs to mainly excrete outdoors, and thus results in improved indoor air quality [6], animal welfare [3], and meat quality [7] compared with a conventional housing system. The design of naturally ventilated pig buildings (NVPBs) with outdoor access is mainly based on the consideration of animal production performance and animal welfare [3,8].

However, one important issue associated with this type of buildings is the amount of air pollutants produced in the buildings and their emission to the surrounding environment. The open-type barn structure allows a direct air exchange between the indoor and outdoor environment, and consequently leads to a wide dispersion of gaseous emissions into the atmosphere [9]. The gaseous pollutants produced from the buildings including ammonia, greenhouse gases, hydrogen sulphide, particulate matter, odours and aerosols contribute to environmental problems and causes nuisance to neighbouring residents [10]. The transport and dispersion processes of gaseous emissions are strongly affected by airflow [11,12], which is influenced by the atmospheric boundary layer (ABL) such as temperature, humidity, wind speed, wind direction, and terrain [13]. The ABL experiences periodic evolution of daytime convective [14], transitional (occurs in the morning, late afternoon or early evening) [15], and nocturnal stable states [16] due to the solar diurnal cycle. This dynamic behaviour of the ABL may also affect the evolution of particulate matter [17]. In addition to the ABL, building configurations (e.g., roof structure and openings) also affect airflow field within and around the building [18], and thus may have an impact on the pollutant transport and dispersion processes. Therefore, a good understanding of airflow distributions including airflow pattern and mean and turbulent characteristics, particularly downwind of the buildings contributes to understanding air pollutant dispersion mechanisms.

One of the most common ways to reduce nuisance of airborne pollutants in the vicinity of pig barns is by using artificial or natural windbreaks [19]. One function of windbreaks is acting as barriers that deflect the airflow upwards, increase the dilution of air pollutants [20], and consequently reduce their concentration at the ground level [21]. Ikeguchi et al. [9] reported that using a solid wall, a screen, and another building as windbreaks placed upwind of a pig barn had different influences on air momentum and airflow patterns around the target building and might affect air dispersion patterns. Apart from the airflow redirection impact, natural windbreaks, for example shelterbelts, also contribute to the reduction of wind speed, interception/absorption of chemical compounds, particulate matter and aerosols, and therefore can dilute and mitigate airborne pollutants [22]. It is found that the influence of natural windbreaks on the pollutant dispersion is related to the height, optical porosity and type of windbreaks [19,20], and the distance from the pollutant source [20,22].

Apart from windbreaks, it is essential to investigate the effect of building configurations e.g., the roof design on the dispersion process of gaseous pollutants. This information may help to provide building engineers guidelines for planning or design of new livestock buildings in order to reduce adverse impacts of the buildings on nearby environment and residents. For environmental reasons, outdoor exercise yards of pig buildings are often partly or totally roofed to minimise the impact of rain to remoisten the soiled areas. Additionally, the roof of a building plays an important role in air separation, airflow pattern within and around the building [23,24] and airflow characteristics in the wake of the building [25], and thus is expected to affect the pollutant dispersion from the building. The effect of building roof on air pollutant transport has been investigated inside and over urban street canyons [26]. It was found that the roof shape [27,28] and the roof slope [28] significantly affected the air vortex within the canyon and the pollutant concentration and dispersion. The influences of the roof type (open-ridge, semi-monitor and mono-slope) and roof slope on air movement for a naturally ventilated dairy house were studied in a wind tunnel, and the dispersion properties were predicted from the airflow measurement results [18]. The authors found that the open-ridge roof type tended to increase dispersion downwind from the house, and the roof slope largely affected the air movement and contaminant dispersion [18]. However, their work only measured air velocities at the vertical symmetry plane of the building, and detailed airflow field information downwind the

building was limited. Moreover, the configurations of NVPBs with roofed outdoor exercise yards are very different from street canyons and dairy houses. There is lack of airflow information about this type of buildings with roofed outdoor exercise areas. Therefore, it is required to understand in detail airflow characteristics including both mean (time-averaged) velocity and turbulent fluctuations downwind NVPBs with outdoor access. This knowledge can contribute to a better understanding of the transport and dispersion processes of airborne pollutants and of an optimised roof design.

Wind tunnel and scaled model experiments are widely applied in aerodynamics studies because of their advantages of allowing fully controlled boundary conditions, working with real airflow [29], providing a large amount of data in a short time [30], and the flexibility in the experimental setup [11]. Because of the scaled-down model, similarity criteria e.g., geometric similarity, boundary similarity, Reynolds number similarity have to be met in order to make the wind tunnel experimental results be comparable to the results from full-scaled buildings [31]. By carefully checking the similarity criteria, the wind tunnel tests method was therefore used in this paper in order to conduct the airflow characteristics research. Moreover, the data obtained from the wind tunnel measurements can also be used to validate accuracy and reliability of computational fluid dynamics (CFD) models and therefore to investigate more complex flow (e.g., airflows above emitting surfaces) and dispersion phenomena, to perform comprehensive parametric studies, and finally to mitigate the production of emissions from livestock buildings.

The objectives of this study were to investigate mean and turbulent characteristics of airflows downwind of a NVPB with an outdoor exercise yard covered with roofs with different roof slopes, to predict air pollutant distribution and dispersion properties, and to provide valuable experimental data for CFD validation. The novelties of this study are as follows:

- It is the first to provide detailed airflow information around a naturally ventilated livestock building combined with a roofed outdoor area;
- It predicts the potential distribution of gaseous pollutants from the building using airflow measurement results;
- It provides a large amount of experimental data of both mean velocity and turbulent fluctuations downwind the building with a high resolution that can be used for CFD validation.

## 2. Materials and Methods

### 2.1. Scaled Pig Building Model

A scaled model of a naturally ventilated pig building with an outdoor exercise yard was used in this study. The prototype pig barn, situated in the state of Lower Saxony in northwest Germany, was designed for rearing around 80 fattening pigs. The scaled model was a 1:50 geometric reduction of the full-scale pig barn and was constructed at the Leibniz Institute for Agricultural Engineering and Bioeconomy (ATB), Germany.

The scaled model was made of transparent acrylic glass and consisted of an indoor housing area and an outdoor exercise area. The external dimension of the model was 0.427 m (length)  $\times$  0.256 m (width)  $\times$  0.130 m (height). The housing area had two sidewall openings with opening heights of 0.020 m and 0.064 m, respectively. Eight pigpens with open pen fronts were placed in the housing area. The height and width of all pigpens were 0.020 m and 0.054 m, respectively. The length of the two pigpens located next to gable walls was 0.056 m, and of other pigpens was 0.050 m. Pigpen walls had a thickness of 0.002 m, and all other walls of the building model had a thickness of 0.003 m. The roof of the building housing area had a fixed slope of 15°. The free access between indoor and outdoor areas through plastic strips or rotating doors in the prototype pig barn was constructed by a 0.025 m high acrylic sheet in the scaled model. The outdoor exercise area had a flexible roof with a length of 0.108 m and with a fixed top part, which totally covered the outdoor yard. There was a 0.010 m high sidewall but were no gable walls in the outdoor area. The prototype pig building was constructed to direct the excretion behaviour of pigs to the outdoor exercise yard [32], in which solid floors in the housing area

and slatted floors with a deep pit in the outdoor area were adopted. Therefore, in this study we only considered the roof slope variations for the outdoor area, where the majority of emissions are expected to come from. Three cases with roof slopes of 5°, 15°, and 25° were studied in this paper. It has been found that the presence of animals has an insignificant impact on the airflow and pollutant dispersion within the barn [33], therefore, pigs and other internal structures that have smaller dimensions than the group of pigs, such as feeders, drinkers, metal bars, and slatted floors are expected to have minor influences on the airflow field downwind of the building. To simplify the model construction, pigs and these internal structures were not constructed. Detailed dimensions of the scaled pig building model and the three roof slope variations are illustrated in Figure 1.

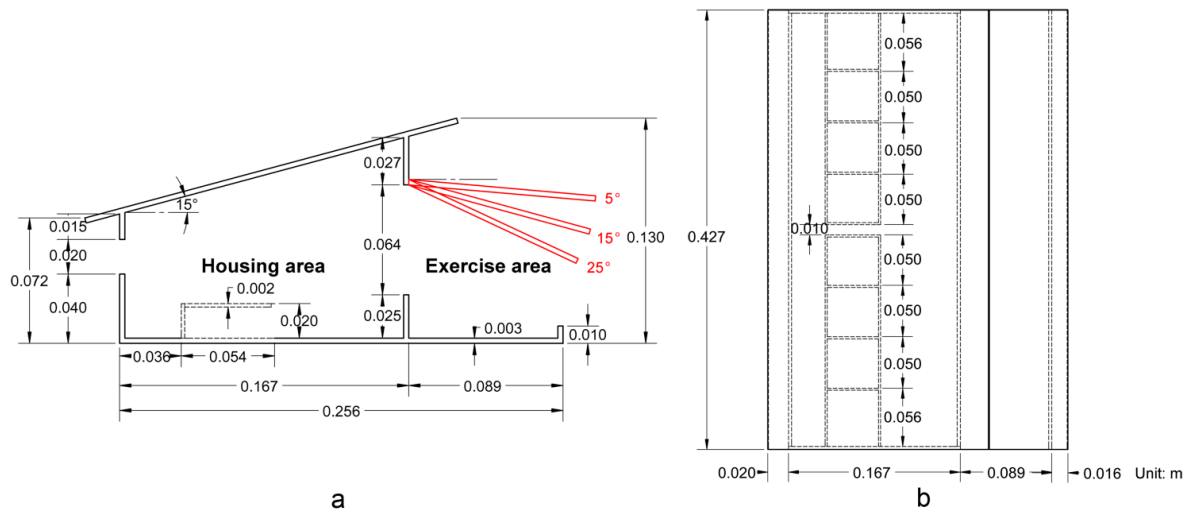


**Figure 1.** Sketch of the 1:50 scaled pig building model. (a) Front view with different slopes of the roof above the exercise yard; (b) top view of the scaled model with 15° roof slope.

## 2.2. Boundary Layer Wind Tunnel and Measurement Devices

The experiments were carried out in a large boundary layer wind tunnel (BLWT) at ATB, Germany. The BLWT was specially designed to investigate ventilation and dispersion processes in agricultural buildings [34–37], and has also been used to generate datasets for CFD validation [24,38,39]. The wind tunnel is 28.5 m long, consisting of an air inlet fitted of honey combs, an air outlet equipped with an axial fan, and a 19.5 m-long test section. The cross-sectional area of the test section is 3 m (width) × 2.3 m (height). A combination of six spires and roughness elements was used to create a boundary layer flow. The spires were installed at the entrance of the test section. The roughness elements consisting of two sizes of right-angled steel brackets, with dimensions length × width × height of 0.010 m × 0.004 m × 0.004 m and 0.004 m × 0.002 m × 0.002 m for small and big brackets respectively, were arrayed in staggered rows downstream the spires. The total length of the roughness elements was 9.6 m with 0.2 m space between each row. The 1:50 scaled pig building model was placed at the symmetry line of the wind tunnel at 1.2 m downstream from the roughness elements. The model was oriented with sidewall openings perpendicular to the approaching flow and the outdoor yard at the downwind side. The blockage ratio of the scaled model to the cross-section of the wind tunnel was 0.8%, which is far less than the recommended maximum value of 5% for wind tunnel tests in VDI-guideline 3783/12 [40], and thus the tunnel effect can be neglected. Figure 2 shows photographs of the wind tunnel with the scaled model placed inside.

The free stream wind speed at the wind tunnel inlet ( $U_{inlet}$ ) was measured using a Prandtl tube, connected to a pressure transducer MKS Baratron® Type 120A (MKS Instruments, Andover, USA). The Prandtl tube was located at the centre of the entrance of the test section at a height of 1.3 m from the wind tunnel floor. Air velocity and turbulence around the scaled model were measured using a 2D fibre-optic Laser Doppler Anemometer (LDA) (Dantec Dynamics, Skovlunde, Denmark) combined

with the BSA Flow Software package (Dantec Dynamics, Skovlunde, Denmark). The LDA probe head was 0.06 m in diameter and 0.45 m in length and provided a focal length of 0.25 m. The LDA probe was mounted on a three-dimensional computer-controlled traverse system that allowed automated and precise probe positioning with an uncertainty of  $<0.1$  mm. A fog generator Tour Hazer II (Smoke Factory, Burgwedel, Germany) was placed at the wind tunnel inlet to produce seeding particles for LDA measurements. The temperature, relative humidity, and static pressure of the ambient air were measured using a FHAD 46x sensor with ALMEMO® D6 plug (AHLBORN Mess- und Regelungstechnik GmbH, Ilmenau, Germany). The data were sampled approximately every hour. The mean values of temperature, relative humidity, and static pressure for each day were used to calculate the air density, and therefore to calculate the  $U_{inlet}$  by using together with the data from the Prandtl tube.

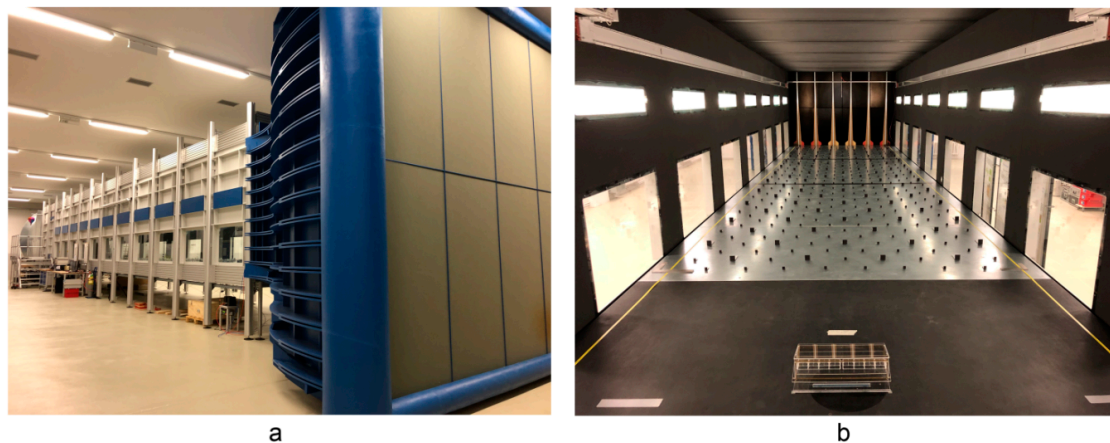


**Figure 2.** Photographs of the boundary layer wind tunnel (BLWT) at the Leibniz Institute for Agricultural Engineering and Bioeconomy (ATB), Germany. (a) Exterior view of the BLWT viewed from the air inlet; (b) interior view of the test section of the BLWT with the 1:50 scaled pig barn model.

### 2.3. Measurement of Boundary Layer Profile

#### 2.3.1. Reynolds Number Independence Study

In order to obtain a fully developed turbulent flow in the wind tunnel, a Reynolds number independence study for the approaching flow was carried out. The wind profile was measured at 20 positions along a vertical line ranging from 0.003 m to 0.6 m above the wind tunnel floor at the upstream edge of the scaled model (i.e., at Line 1 in Figure 3). The wind profile measurements were performed without the presence of the scaled model at free stream wind speeds ( $U_{inlet}$ ) of 4, 6, 8, 10, and 12  $\text{m}\cdot\text{s}^{-1}$ , respectively. The streamwise ( $U$ ) and vertical ( $W$ ) velocity components were measured using the 2D LDA. The measurements at each measurement position were taken continuously until the sampling number reached 40,000 readings or the maximum sampling time reached 820 s before moving the LDA probe to another position. The average sampling rate during experiments was around 300  $\text{s}^{-1}$ . A 10s pause between each measurement position was set in order to minimise the disturbance of the movement of the LDA probe to the flow field. The above LDA setup was chosen according to a preliminary experiment for the reproducibility of statistic results, in which air velocities at heights of 0.01 m, 0.03 m, 0.06 m, 0.1 m, and 0.2 m along Line 1 were measured and repeated three times at  $U_{inlet}$  of 8  $\text{m}\cdot\text{s}^{-1}$ . The results showed that with this setup the measurement uncertainty for the time-averaged  $U$  and  $W$  velocities was 0.3%, and 5.5%, respectively (Figure 4). The above mentioned LDA setup was used for all air velocity measurements in this study.

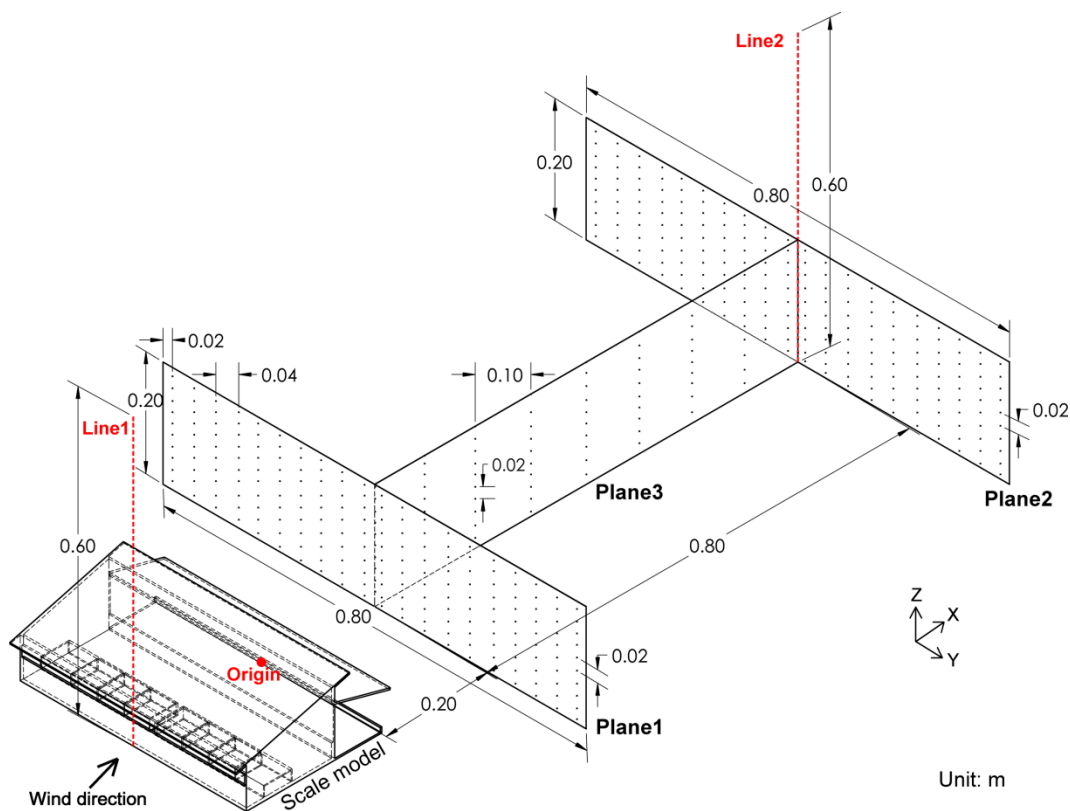


**Figure 3.** Isometric view of the scale model and air velocity measurement positions. Lines 1 and 2 indicate vertical lines for wind profile measurements. The black dots at Planes 1–3 represent actual velocity measurement positions downwind the building. X, Y and Z represent axes of the coordinate system. The red dot represents the origin of the coordinate system.

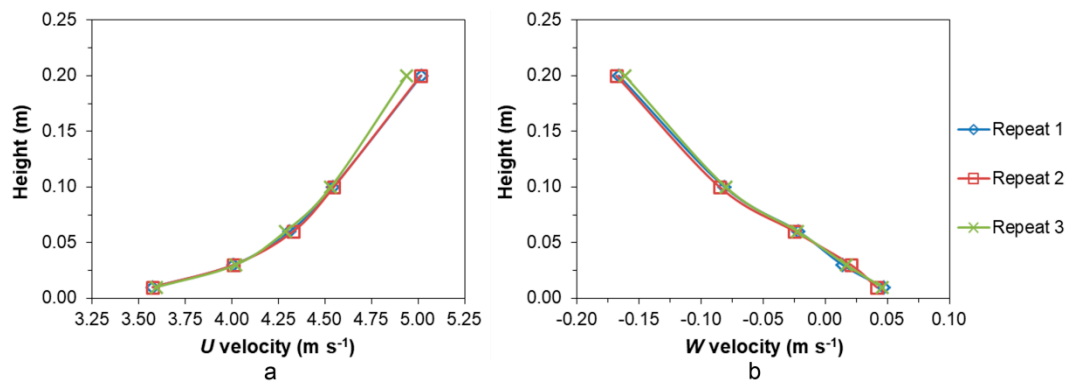


**Figure 4.** Reproducibility study for air velocity measurements in the wind tunnel without scaled model for free stream wind speed of  $8 \text{ m}\cdot\text{s}^{-1}$ . (a) and (b) represent streamwise ( $U$ ) and vertical ( $W$ ) air velocity components, respectively.

### 2.3.2. Stability Study

To establish a stable boundary layer airflow that represents a farmland terrain, the characteristics of wind profiles within the region of interest were assessed. The arrangement of the roughness elements was adjusted accordingly until reaching a desirable boundary layer flow following the VDI-guideline 3783/12 [40]. Air velocities at two vertical lines, one at the upstream edge of the scaled model (i.e., Line 1 in Figure 3) and the other at the downstream end of the region of interest (i.e., Line 2 in Figure 3), from 0.003 m to 0.6 m height along the symmetry line of the model were measured. Measurements were carried out using the 2D LDA without the presence of the scaled model. Free stream wind speed

in the wind tunnel was  $8 \text{ m}\cdot\text{s}^{-1}$ . Parameters that define the roughness class of the boundary layer, e.g., the wind profile power exponent, roughness length, and turbulence intensity were examined.

#### 2.4. Measurement of Airflows Downwind the Building

In order to investigate airflow characteristics and to predict air pollutant dispersion properties downwind the building, air velocities at three vertical planes (Planes 1–3, Figure 3) downwind the 1:50 scaled pig building model were measured with the LDA. Streamwise and vertical velocity components were measured simultaneously. Mean and instantaneous air velocities were recorded to obtain average and turbulent airflow information. Plane 1 and Plane 2 were parallel to the building sidewalls at separation distances of 0.2 m (corresponded to 10 m in full-scale) and 1.0 m (corresponding to 50 m in full-scale) downwind the building model, respectively. Both Plane 1 and Plane 2 had a dimension of  $Y \times Z = 0.8 \text{ m}$  (width)  $\times 0.2 \text{ m}$  (height), each consisting of 200 velocity measurement points with 10 points in each vertical line and 20 points in each horizontal line. Plane 3 was positioned along the symmetry plane of the scaled model with a dimension of  $X \times Z = 0.8 \text{ m}$  (length)  $\times 0.2 \text{ m}$  (height), including 90 measurement positions distributed at 9 vertical lines. In this study,  $X$ ,  $Y$  and  $Z$  denoted the axes of the coordinate system, which were aligned with the streamwise, spanwise and vertical wind directions, respectively. The origin of the coordinate system was located at the centre of the downstream edge of the scaled model at the wind tunnel floor. The airflow measurement positions and the definition of the coordinate system are depicted in Figure 3. According to the wind profile measurement results (described in Section 3.1), a stable and fully developed turbulent flow that represents a farmland terrain boundary layer could be obtained when the free stream wind tunnel speed ( $U_{inlet}$ ) was at least  $8 \text{ m}\cdot\text{s}^{-1}$ . Therefore, all airflow measurements downwind the scaled model were performed at  $U_{inlet}$  of  $8 \text{ m}\cdot\text{s}^{-1}$ .

#### 2.5. Data Analysis

The mean and the standard deviation of the air velocity in streamwise and vertical directions at each measurement position were provided by BSA Flow Software (Dantec Dynamics, Skovlunde, Denmark). Air velocity and air turbulence characteristics were processed from 40,000 samples at each position to ensure statistically reliable results.

The velocity magnitude calculated from two-dimensional velocity components was defined as:

$$V_{2D} = \sqrt{U^2 + W^2} \quad (1)$$

where  $V_{2D}$  is the velocity magnitude,  $\text{m}\cdot\text{s}^{-1}$ ;  $U$  and  $W$  are mean air velocities in streamwise and vertical directions, respectively,  $\text{m}\cdot\text{s}^{-1}$ .

Turbulence intensity and turbulent kinetic energy of the airflow were calculated by Equations (2) and (3), respectively.

$$TI = \sqrt{0.5(\sigma_U^2 + \sigma_W^2)} / V_{2D} \times 100\% \quad (2)$$

$$TKE = 0.5(\sigma_U^2 + \sigma_W^2) \quad (3)$$

where  $TI$  is the turbulence intensity, %;  $TKE$  is the turbulent kinetic energy,  $\text{m}^2\cdot\text{s}^{-2}$ ;  $V_{2D}$  is the velocity magnitude,  $\text{m}\cdot\text{s}^{-1}$ ;  $\sigma_U$  and  $\sigma_W$  are standard deviations of the instantaneous air velocity in streamwise and vertical directions, respectively,  $\text{m}\cdot\text{s}^{-1}$ .

It is noted that in this study  $V_{2D}$ ,  $TI$ , and  $TKE$  were calculated based on a two-component velocity analysis.

### 3. Results and Discussion

#### 3.1. Boundary Layer Profile

##### 3.1.1. Reynolds Number Independence Study

Dimensionless streamwise ( $U/U_{inlet}$ ) and vertical ( $W/U_{inlet}$ ) velocity profiles in the vertical direction ( $Z$ ) at Line 1 in Figure 3 are compared in Figure 5 for different free stream wind speeds at the wind tunnel inlet ( $U_{inlet}$ ), in order to identify the critical  $U_{inlet}$  above which the flow can be considered Reynolds number independent [41]. The results showed that under  $U_{inlet}$  of  $4 \text{ m}\cdot\text{s}^{-1}$  and  $6 \text{ m}\cdot\text{s}^{-1}$  conditions, the values of both  $U/U_{inlet}$  and  $W/U_{inlet}$  were different to the other cases. When  $U_{inlet}$  increased from  $6 \text{ m}\cdot\text{s}^{-1}$  to  $8 \text{ m}\cdot\text{s}^{-1}$ , the average relative change of dimensionless air velocities was 0.391 and 0.006 for  $U/U_{inlet}$  and  $W/U_{inlet}$ , respectively. In contrast, when  $U_{inlet}$  increased from  $8 \text{ m}\cdot\text{s}^{-1}$  to  $10 \text{ m}\cdot\text{s}^{-1}$ , the average relative change was only 0.003 and 0.001 for  $U/U_{inlet}$  and  $W/U_{inlet}$ , respectively. It indicated that when  $U_{inlet}$  exceeded  $8 \text{ m}\cdot\text{s}^{-1}$ , the dimensionless wind profile did not change considerably with further increase of the wind tunnel wind speed. Therefore, the Reynolds number independence was reached and a fully-developed turbulent flow was obtained at  $U_{inlet}$  of  $8 \text{ m}\cdot\text{s}^{-1}$ .

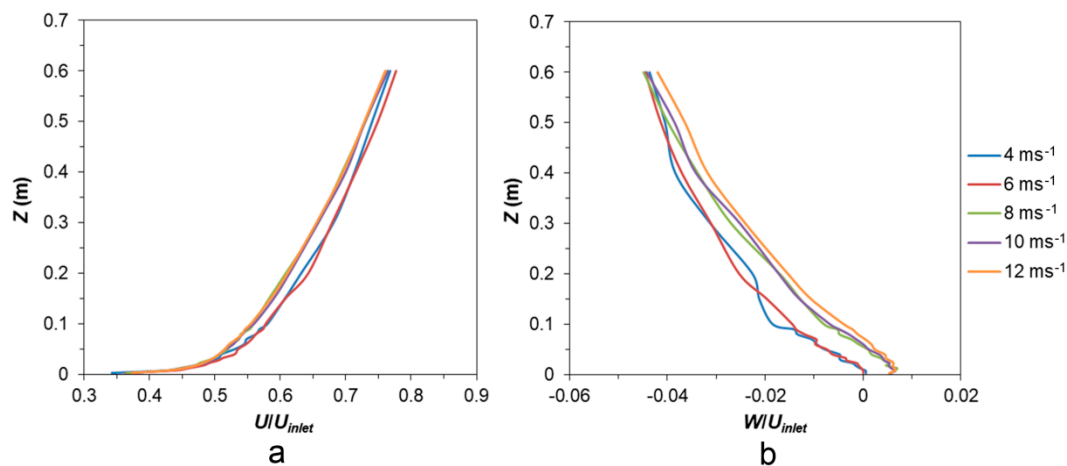


**Figure 5.** Dimensionless streamwise ( $U/U_{inlet}$ ) (a) and vertical ( $W/U_{inlet}$ ) (b) air velocity profiles of the incident flow in the vertical direction ( $Z$ ) at the wind tunnel inlet wind speed ( $U_{inlet}$ ) of 4, 6, 8, 10, and 12  $\text{m}\cdot\text{s}^{-1}$ .

##### 3.1.2. Stability Study and Wind Profile Properties

To ensure a stable airflow within the region of interest, wind profiles at the upwind edge of the model (Line1) and the end of downwind airflow measurement region (Line 2) were measured without the scaled model. The vertical profiles of the streamwise air velocity component for Line 1 and Line 2 are compared in Figure 6. The results showed that the two profiles agreed well with each other with an average relative difference of 3.5%, indicating that a stable airflow was achieved within the region of interest.

Figure 6 showed that the mean streamwise air velocity profile of the incident flow (i.e., at the upwind edge of the model) in the vertical direction followed a power law with the exponent of 0.14 and the coefficient of determination  $R^2$  of 0.98:

$$U = U_{ref} \left( Z / Z_{ref} \right)^{0.14} \quad (4)$$

where  $U$  and  $U_{ref}$  are the mean streamwise air velocity at height  $Z$  and a reference height  $Z_{ref}$ , respectively,  $\text{m}\cdot\text{s}^{-1}$ . To achieve the best fit of the model for the air velocity profile,  $U_{ref} = 5.55 \text{ m}\cdot\text{s}^{-1}$  and  $Z_{ref} = 0.4 \text{ m}$  were chosen in this study.

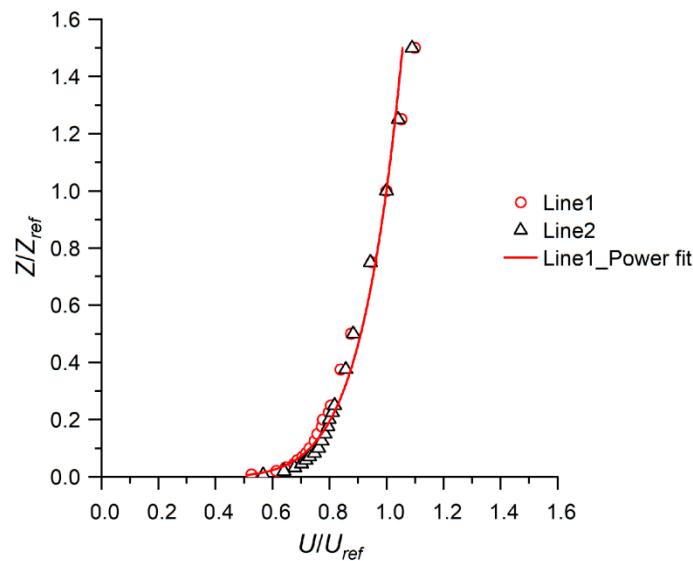


**Figure 6.** Comparison of vertical ( $Z$ ) profiles of streamwise air velocity ( $U$ ) measured at Line 1 and Line 2.  $U_{ref}$  is the reference streamwise velocity at the reference height  $Z_{ref}$ . The red line is the power fit of the wind profile measured at Line 1.

The streamwise air velocity at the building height ( $U_B$ ), calculated by Equation (4), was  $4.77 \text{ m}\cdot\text{s}^{-1}$ . This resulted in a building Reynolds number ( $Re_B$ ) of 53,759, which was calculated by Equations (5) and (6).

$$Re_B = U_B \cdot D / \nu \tag{5}$$

$$D = 2W_B \cdot Z_B / (W_B + Z_B) \tag{6}$$

where  $\nu$  is the kinematic viscosity of the air,  $\text{m}^2\cdot\text{s}^{-1}$ ;  $D$  is the characteristic length of the scaled pig building model, calculated as the hydraulic diameter of the cross-section of the model, m;  $W_B$  and  $Z_B$  are the width and the height of the scaled model, respectively, m. The average ambient temperature and relative humidity during the whole experimental period were  $22.4 \text{ }^\circ\text{C}$  and 34.2%, respectively. Therefore,  $\nu$  took the value of  $1.53 \times 10^{-5} \text{ m}^2\cdot\text{s}^{-1}$  at temperature of  $22.4 \text{ }^\circ\text{C}$ .

By fitting the air velocity profile of the incident flow to a logarithmic law, it gave the friction velocity ( $u^*$ ) of  $0.22 \text{ m}\cdot\text{s}^{-1}$  and the full-scale roughness length ( $z_0$ ) of  $6.4 \times 10^{-3} \text{ m}$ , in which the von Karman constant took the value of 0.4. This gave the roughness Reynolds number ( $Re_{z_0}$ ) of 92, which was calculated according to Equation (7).

$$Re_{z_0} = u^* \cdot z_0 / \nu \tag{7}$$

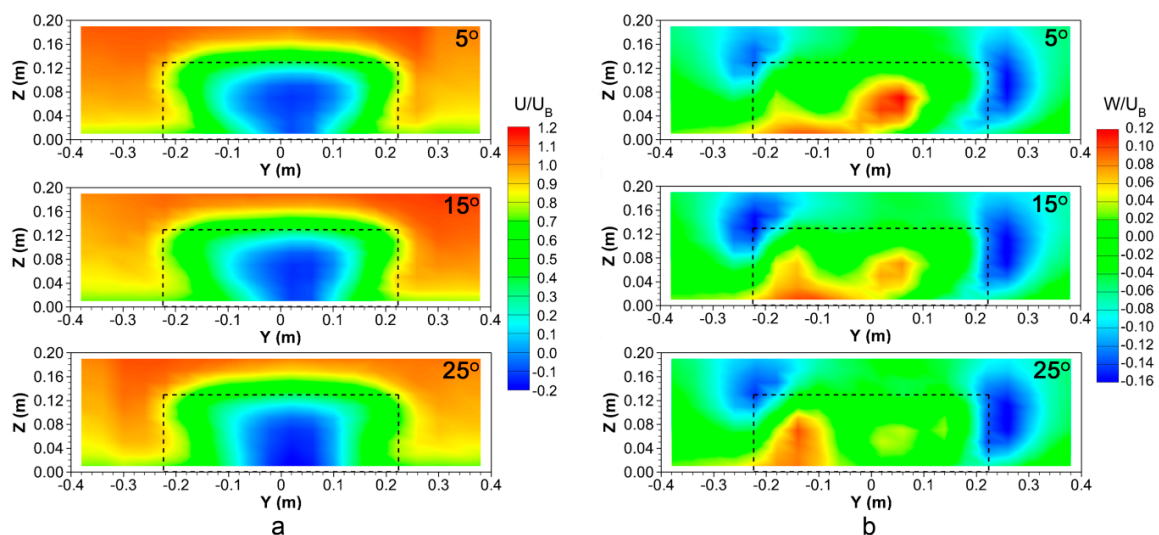
It is stated in the VDI-guideline [40] that a moderately rough (corresponds to grassland or farmland) turbulent boundary layer should meet the following requirements: the profile power law exponent falls within the region of 0.12–0.18, and the roughness length within 0.005–0.1 m. In this study, both the power exponent of 0.14 and  $z_0$  of  $6.4 \times 10^{-3} \text{ m}$  satisfied the aforementioned criteria, hence the generated boundary layer can be considered to represent the airflow over farmland terrain.

Additionally, both the building Reynolds number ( $Re_B$ ) of 53,759 and the roughness Reynolds number ( $Re_{z_0}$ ) of 92 were considerably higher than the reported critical  $Re_B$  of 4000 [42] and critical  $Re_{z_0}$  of 2.5 [43], respectively for a Reynolds number independent flow. It further indicated that the airflow generated in our wind tunnel at  $U_{inlet}$  of  $8 \text{ m}\cdot\text{s}^{-1}$  was fully developed turbulent.

Therefore, all subsequent measurements were performed at  $U_{inlet}$  of  $8 \text{ m}\cdot\text{s}^{-1}$ .

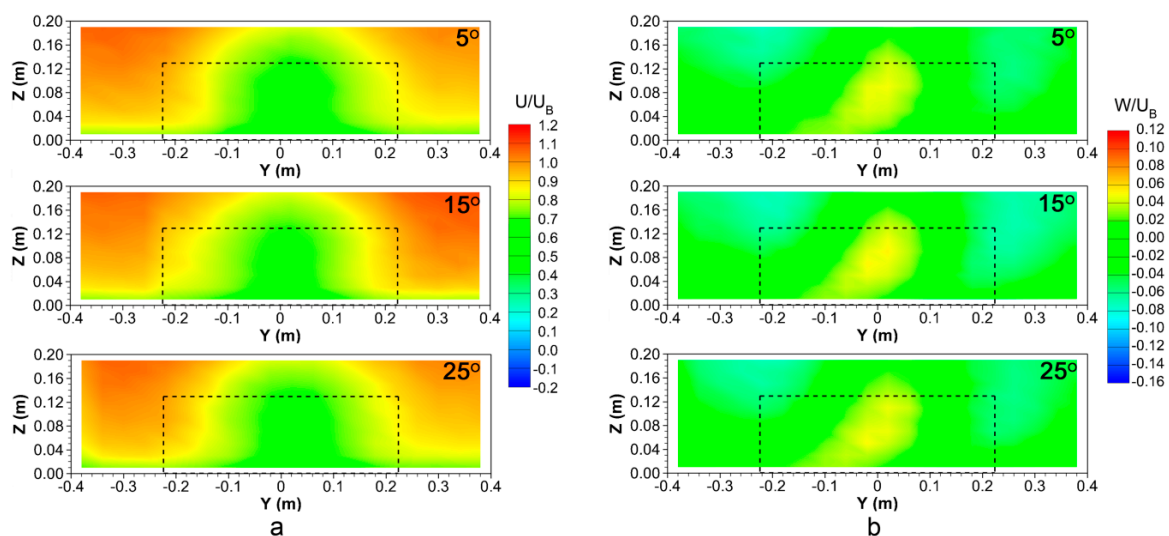
### 3.2. Mean Air Velocities Downwind the Building

Figure 7a shows contours of mean streamwise air velocity normalised by the air velocity at the building height ( $U_B$ ) at Plane 1 for three roof slopes of the exercise yard of the scaled pig building model. Considerably lower air velocities were observed right behind the building with negative values in the centre (represented in dark blue in Figure 7a). The negative  $U$  velocities indicated reverse flows through Plane 1, which occurred slightly below the building height. The region of the reverse flow was affected by the roof slope in the spanwise wind direction ( $Y$ ). It became narrower in the upper part but wider in the lower part for a steeper roof. Beyond the reverse flow region, the air flowed towards downstream with a reduced air velocity. Figure 7b compares the dimensionless mean vertical air velocity contours at Plane 1 for roof slopes of  $5^\circ$ ,  $15^\circ$ , and  $25^\circ$ . It was found that at both sides of the building,  $W$  velocities were negative, which indicated a downward flow direction. In contrast, within the region right behind the building upward airflows were observed. This indicated a complex three-dimensional air movement downwind the building caused by the air passing through and around the building. It is noted that the velocity contours were not strictly symmetric even though the scaled model was geometrically symmetric and the wind direction was perpendicular to the model sidewalls. The most possible reason for the asymmetrical airflow contours was the disturbance of the LDA probe to the flow field when it was positioned close to the building. The cross-sectional area of the LDA probe was  $0.003 \text{ m}^2$ , accounting for 5% blockage to the airflow at the position right behind the building. This was not intended but was unavoidable, restricted by the focal length of the LDA. The potential influence of the air velocity sensor to the airflow was also reported by Sauer et al. [25], who observed an asymmetrical air velocity pattern at a vertical plane downstream from four aligned swine building models measured using a 3D hot-film anemometer. The results raised a potential interesting topic that is to quantify the disturbance of the LDA probe to the flow field, which could be done with CFD simulations.



**Figure 7.** Spatial distributions of (a) streamwise ( $U$ ) and (b) vertical ( $W$ ) air velocities at Plane 1 for roof slopes of  $5^\circ$ ,  $15^\circ$ , and  $25^\circ$ .  $U_B$  is the streamwise air velocity at the building height. Black dash lines indicate the profile of the scaled model.

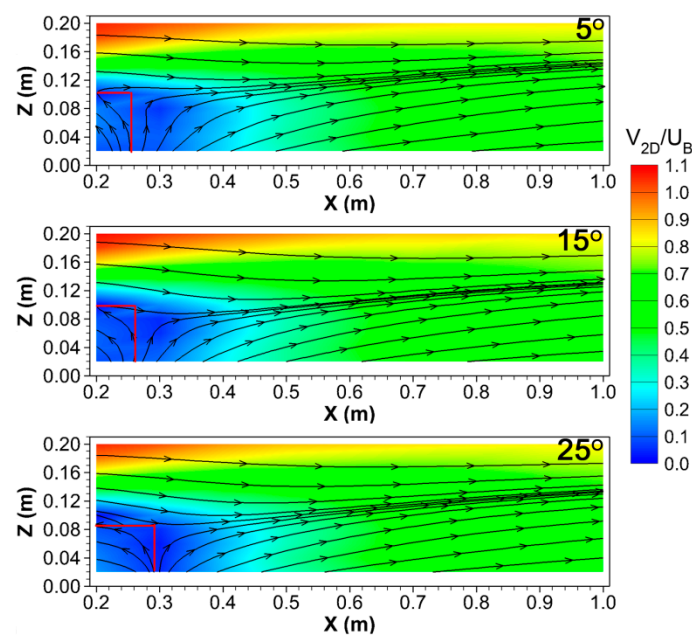
Figure 8 depicts contours of dimensionless streamwise and vertical air velocities at Plane 2 for the three roof slopes. Lower air velocities at the position behind the building than around the building were still observed. This indicated that the presence of the building affected the airflow field at a distance of 1.0 m (i.e.,  $7.7Z_B$ , where  $Z_B$  is the building height, corresponding to 50 m in full scale) downwind the building. In contrast to Plane 1, no reverse flows occurred at Plane 2 for all three cases. It was found that  $U$  velocities right behind the building at Plane 2 were obviously higher than those at Plane 1. However, Plane 1 presented higher air velocities at the height above 0.16 m than Plane 2 (Figures 7a and 8a), which was caused by the wind shear effect that accelerated the air when the air flowed over the top of the building. Compared with Plane 1, Plane 2 presented a more homogeneous vertical air velocity pattern with slightly upward airflows occurring near the centre (Figure 8b). Only small differences among different roof slope cases for both  $U$  and  $W$  velocities at Plane 2 were observed. It demonstrated that the slope of the leeward roof did not considerably affect the airflow at Plane 2.



**Figure 8.** Spatial distributions of (a) streamwise ( $U$ ) and (b) vertical ( $W$ ) air velocities normalised by the air velocity at building height ( $U_B$ ) at Plane 2 for roof slopes of  $5^\circ$ ,  $15^\circ$ , and  $25^\circ$ . Black dash lines indicate the profile of the scaled model.

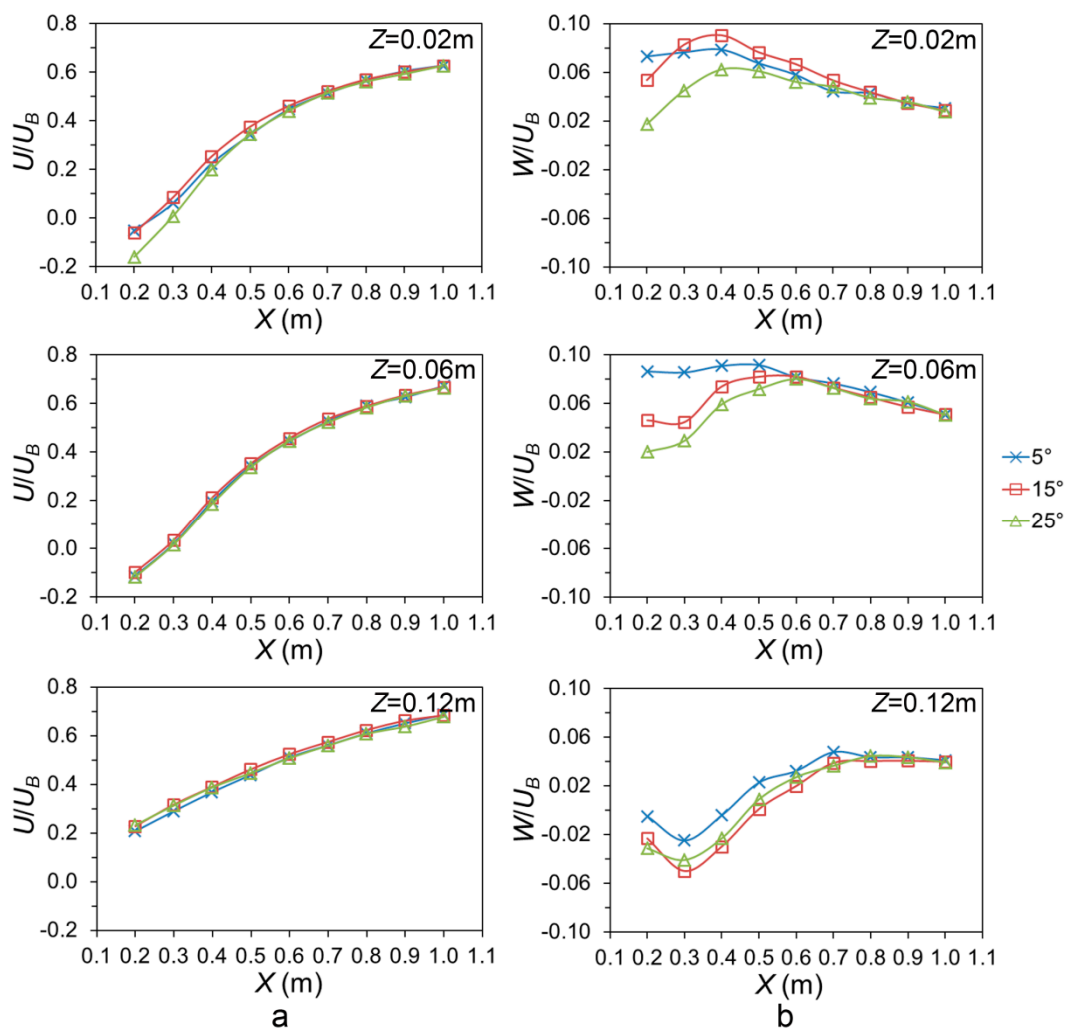
Airflow streamlines and contours of the air velocity magnitude ( $V_{2D}$ ) normalised by  $U_B$  at Plane 3 for the three roof slopes are compared in Figure 9. The axes  $X$  and  $Z$  indicate the downwind distance to the building and the height from the wind tunnel floor, respectively. There was an elliptic-shaped low air velocity region with  $V_{2D}/U_B$  of smaller than 0.4 behind the building with a height of 0.13 m (i.e.,  $1Z_B$ ) and a downstream distance of 0.5 m (i.e.,  $3.8Z_B$  and corresponding to 25 m in full-scale) for all three roof slopes. This region is expected to have a high concentration of air pollutants. This is because airborne pollutants are mainly transported by mean airflow, which results in the concentration of pollutants being inversely related to the air velocity downwind the building if no recirculation regions are presented [44]. If applying additional air pollutant treatment technologies, for example using pollutant traps or sprinklers to collect or wash high-concentrated air pollutants in this low air velocity region might effectively mitigate air contaminants and release their burden to the surrounding environment and residents. Additionally, within this low air velocity region, a wake zone with reversed airflow was observed at Plane 3, implying an anti-clockwise air recirculation in which air pollutants would accumulate. The size and shape of the wake was affected by the roof slope. For the roof slope of  $5^\circ$ ,  $15^\circ$ , and  $25^\circ$ , the wake height (in  $Z$  direction) was 0.103 m, 0.099 m, and 0.084 m, respectively. Accordingly, the wake length (in  $X$  direction) was 0.254 m, 0.261 m, and 0.290 m, respectively. It showed that the larger the roof slope was, the lower and longer the wake became, and vice versa. As a result, the accumulated air pollutants would disperse farther for a steeper roof slope. The wake length

observed by Tominaga et al. [23] was  $2.5Z_B$  and  $2.8Z_B$  for a gable-roof building (without openings) with the roof slope of  $16.7^\circ$  and  $26.6^\circ$ , respectively, which is slightly greater than  $2.0Z_B$  and  $2.2Z_B$  for the roof slope of  $15^\circ$  and  $25^\circ$  respectively obtained in our study. This is because the sealed building structure could result in a much lower pressure field behind the building and thus a larger air recirculation region. In contrast to the results in this paper where the wakes were found from the floor level until above the roof, in a wind tunnel study of Ikeguchi and Okushima [18] using naturally ventilated dairy building models without outdoor exercise yards, the wakes were only observed above the leeward roof. One possible reason could be the large sidewall openings used in their study, which resulted in a cross ventilation through the building. In contrast, in our study, a small slot inlet opening with a high sidewall led to an up-jet airflow pattern inside the housing area. Additionally, the exercise yard with an upwind sidewall further complicated the airflow and resulted in the reversed flow behind the building. Therefore, our results are expected to be applicable to naturally ventilated livestock buildings with small inlet openings and downwind outdoor yards in a perpendicular wind direction.



**Figure 9.** Air streamlines with contours of normalised air velocity magnitude ( $V_{2D}/U_B$ ) at Plane 3 for roof slopes of  $5^\circ$ ,  $15^\circ$ , and  $25^\circ$ .  $U_B$  is the streamwise air velocity at the building height. Red lines indicate the height and length of the wake for each case.

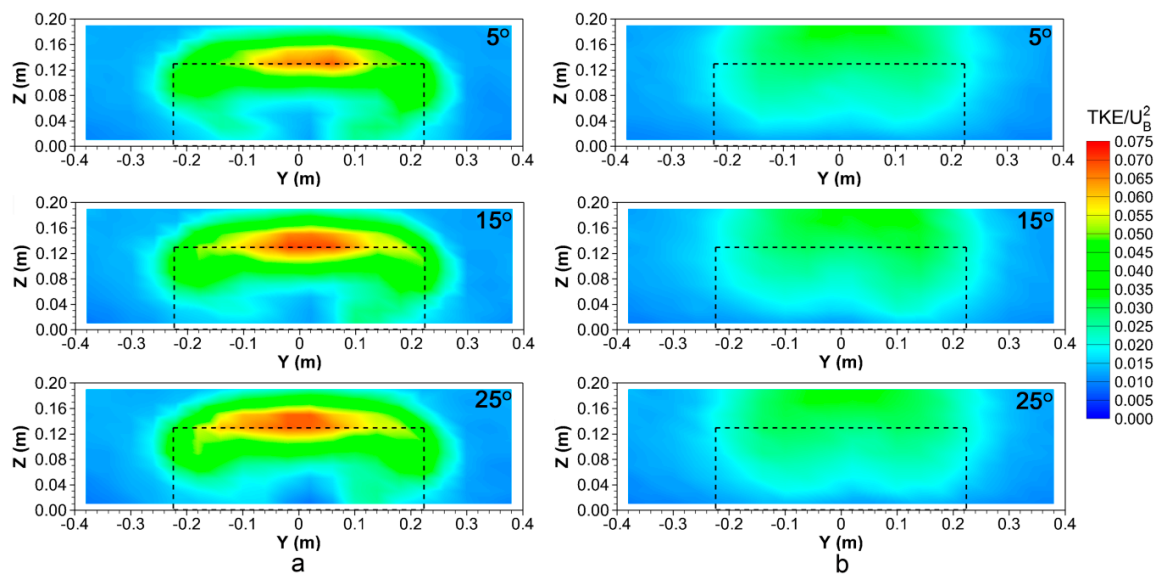
Figure 10 shows the variations of the dimensionless air velocities with distance to the building at heights ( $Z$ ) of 0.02 m, 0.06 m, and 0.12 m, which corresponded to 1 m, 3 m, and 6 m in full-scale. At  $Z$  of 0.02 m, the roof slope of  $25^\circ$  resulted in lower  $U/U_B$  and  $W/U_B$  velocities than roof slopes of  $5^\circ$  and  $15^\circ$  until a distance of around 0.7 m from the building. At  $Z$  of 0.06 m and 0.12 m, there were not many differences for  $U/U_B$  velocities among the three roof slopes. However, for  $W/U_B$  velocities, the  $5^\circ$  roof slope presented the highest values among three cases until a distance of 0.6 m at  $Z$  of 0.06 m and a distance of 0.8 m at  $Z$  of 0.12 m, respectively, indicating a more upwards airflow direction. At a distance beyond 0.8 m (i.e.,  $6.2Z_B$ ) from the building, the roof slope had almost no effect on the air velocities. This is in line with the previous observations at Plane 2 shown in Figure 8 where no considerable differences could be detected among three roof slope cases.



**Figure 10.** Variations of normalised streamwise air velocity  $U/U_B$  (a) and vertical air velocity  $W/U_B$  (b) with respect to the distance from the building ( $X$ ) at heights ( $Z$ ) of 0.02 m, 0.06 m, and 0.12 m for roof slopes of  $5^\circ$ ,  $15^\circ$ , and  $25^\circ$ .  $U_B$  is the streamwise air velocity at the building height.

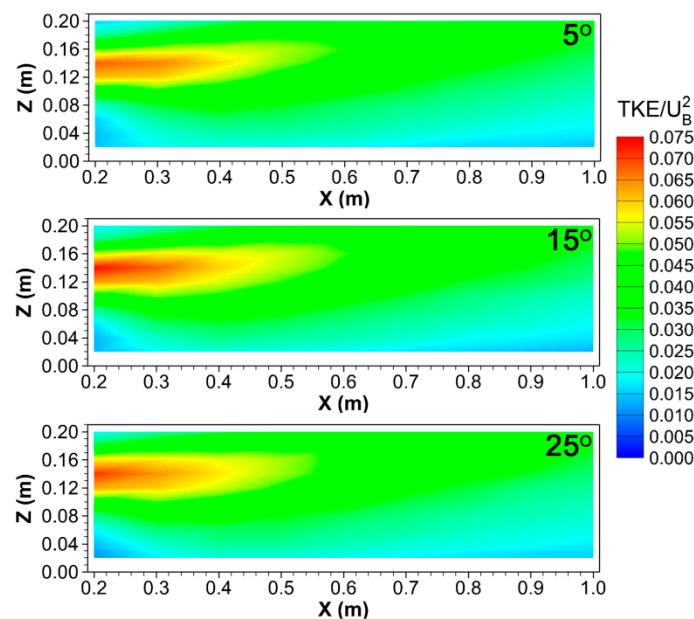
### 3.3. Air Turbulence Downwind the Building

Spatial distributions of the turbulent kinetic energy ( $TKE$ ) normalised by the square of the streamwise air velocity at the building height ( $U_B$ ) at Plane 1 and Plane 2 for roof slopes of  $5^\circ$ ,  $15^\circ$ , and  $25^\circ$  are compared in Figure 11. It was found that  $TKE$  had different patterns from air velocities, where the region of low air velocities generally presented higher  $TKE$  values. At Plane 1, the highest  $TKE$  occurred at the centre of the building around the building height. This might be caused by the air collision of the reverse flow occurred in the wake and the bulk air flowed over the building, which increased the air turbulence in that region. At Plane 1, the high  $TKE$  region was the smallest when the roof slope was  $5^\circ$ . At Plane 2, higher  $TKE$  was observed behind and above the building than in other areas. It indicated that the influence of the building on the downwind air turbulence reached Plane 2. Only minor  $TKE$  pattern differences among different roof slopes were observed at Plane 2, which implied that the roof slope had almost no effects on  $TKE$  at Plane 2.



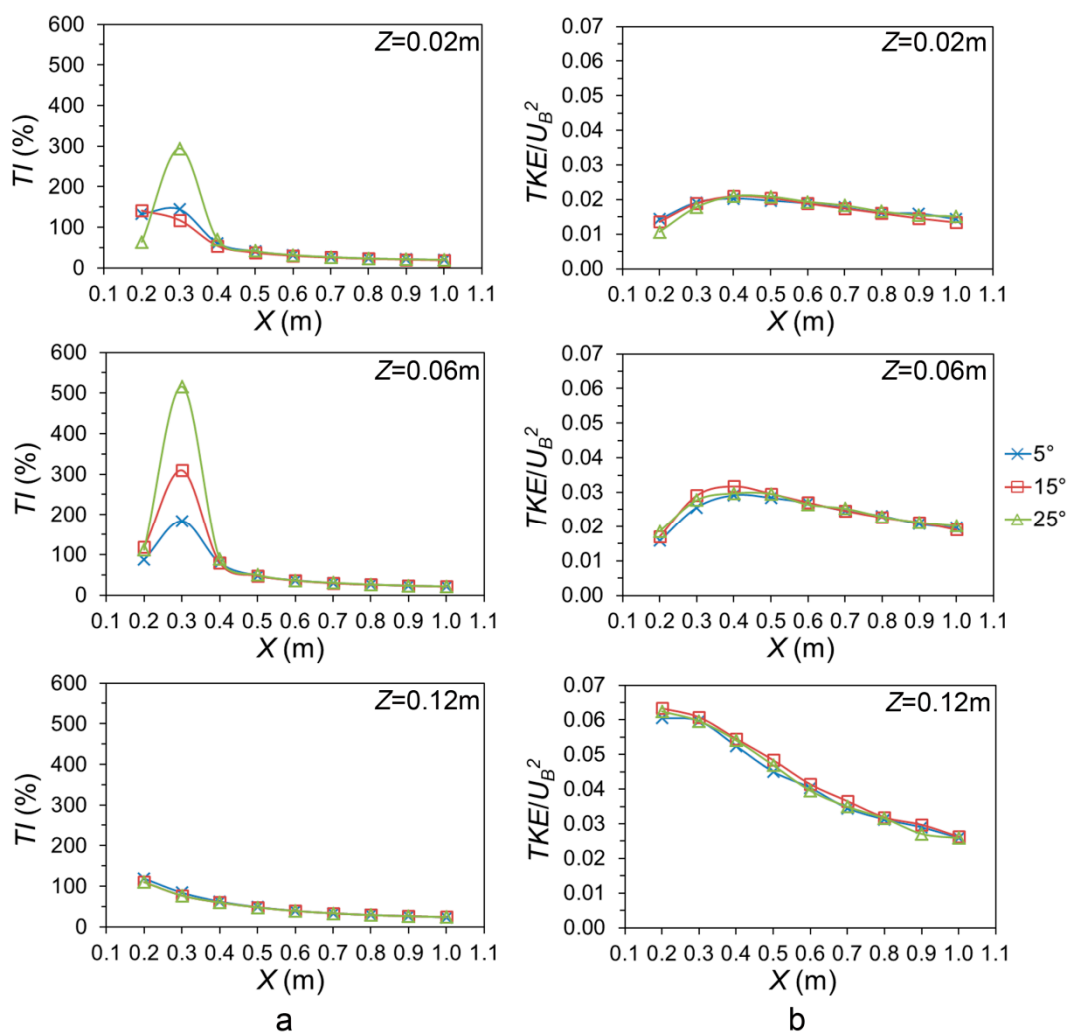
**Figure 11.** Spatial distributions of turbulence kinetic energy ( $TKE$ ) normalised by the square of the air velocity at the building height ( $U_B^2$ ) at Plane 1 (a) and Plane 2 (b) for roof slopes of  $5^\circ$ ,  $15^\circ$ , and  $25^\circ$ . Black dash lines indicate the profile of the scaled model.

Figure 12 illustrates the normalised  $TKE$  distributions at Plane 3 for three roof slopes. The highest  $TKE$  was observed in the region in the vicinity of the building height. It decayed gradually as the distance to the building increased. The high  $TKE$  region that is represented in red and yellow in Figure 12 extended up to approximately 0.5 m (i.e.,  $3.8Z_B$ ) downwind from the building. It was located right above the region in which the air velocity was low (as depicted in Figure 9). This could be attributed to the flow reattachment on the leeward roof that led to the production of  $TKE$ . Ntinis et al. [45] also found a high turbulence production in the air recirculation region behind the scaled model. It is known that the transport of airborne pollutants is affected by both the mean air velocity and the air turbulence [46]. Therefore, in that low air velocity region, the aerial pollutants would be likely transported via the energetic turbulent eddies/turbulence diffusion.



**Figure 12.** Dimensionless turbulence kinetic energy ( $TKE/U_B^2$ ) distributions at Plane 3 for roof slopes of  $5^\circ$ ,  $15^\circ$ , and  $25^\circ$ .

The influences of the roof slope on the air turbulence, denoted by the turbulence intensity ( $TI$ ) and dimensionless turbulent kinetic energy ( $TKE/U_B^2$ ), with respect to the downwind distance from the building ( $X$ ) at heights ( $Z$ ) of 0.02 m, 0.06 m, and 0.12 m are described in Figure 13. A considerably higher  $TI$  was found at  $X$  of 0.2 m–0.4 m for  $Z$  of 0.02 m and 0.06 m, where the air vortex was formed in the wake as depicted in Figure 9. The highest  $TI$  was observed in the most downward roof structure (i.e., roof slope of  $25^\circ$ ), which was attributed to an enhanced disturbance of the roof to the airflow. At  $Z$  of 0.12 m, the  $TI$  had lower values compared with  $Z$  of 0.02 m and 0.06 m, and decreased slowly with distance from the building. The influence of the roof slope on the  $TI$  was negligible when the distance from the building exceeded 0.5 m (i.e.,  $3.8Z_B$ ) (Figure 13a). The highest  $TKE/U_B^2$  occurred at  $Z$  of 0.12 m and decayed gradually away from the building. Even though the roof slope had a big impact on the  $TI$ , no notable differences were observed among different roof slope cases for  $TKE/U_B^2$ , indicating that the variations in the leeward roof slope might have little influence on the turbulent kinetic energy of the airflow downwind the building. The same  $TKE/U_B^2$  values for different cases implied that the velocity fluctuations, as explained by Equation (3), were not affected by the roof slope. However, the velocity magnitude ( $V_{2D}$ ), which was calculated from the  $U$  and  $W$  velocities (Equation (1)) were affected by the roof slope, as seen in Figure 10. According to Equation (2),  $TI$  was calculated as the ratio of the square root of  $TKE$  to  $V_{2D}$ . Therefore, different  $TI$  values were observed among different roof slope cases although the same  $TKE/U_B^2$  occurred.



**Figure 13.**  $TI$  (a) and  $TKE/U_B^2$  (b) variations with respect to the distance to the building ( $X$ ) at heights ( $Z$ ) of 0.02 m, 0.06 m, and 0.12 m for roof slopes of  $5^\circ$ ,  $15^\circ$ , and  $25^\circ$ .

#### 4. Conclusions

Mean air velocity and air turbulence downwind a 1:50 scaled model of a naturally ventilated pig building with a totally roofed outdoor exercise yard with different roof slopes were measured in a large boundary layer wind tunnel to investigate downwind airflow characteristics and the related air pollutant transport and dispersion properties. Before the downwind airflow measurements, wind profile properties were examined to ensure a fully-developed turbulent flow in the wind tunnel. Based on the results obtained, the following conclusions could be drawn:

1. Reduced air velocities were observed right behind the building. At the vertical plane parallel to the building sidewalls with a distance 0.2 m (i.e.,  $1.5Z_B$ , where  $Z_B$  is the building height) downwind the building, reverse flows occurred in the centre of the plane and were affected by the roof slope.
2. An elliptic-shaped low air velocity region along the distance to the building was found. It had a similar height as the building and reached 0.5 m (i.e.,  $3.8Z_B$  and corresponded to 25 m in full-scale) downwind from the building. Within this region, the mean air velocities were low and thus might result in a higher gaseous pollutant concentration. This suggested that applying additional treatment technologies to trap the high-concentrated gaseous pollutants (e.g., odours or ammonia) in this region might contribute to the mitigation of pollutant emissions to the atmosphere and alleviation of the burden to the surrounding environment. Apart from the mean air velocity, the transport of the air pollutants in this region was likely attributed to the turbulent eddies.
3. A wake zone with recirculated air was observed for all three roof slope cases. The larger the roof slope was, the lower and longer the wake zone became. It indicated that a steeper roof could result in the accumulated air pollutants dispersing to a farther distance.
4. The effect of the roof slope to the mean air velocity and the air turbulence could reach up to distances of 0.8 m (i.e.,  $6.2Z_B$ ) and 0.5 m (i.e.,  $3.8Z_B$ ) downwind from the building, respectively.

To the best of our knowledge, the present study was the first to provide detailed information of the downwind airflow for a naturally ventilated pig building with totally roofed outdoor access. The airborne pollution transport and dispersion properties were predicted from the airflow characteristics. To support the findings, further research on the downwind gas concentration fields using a tracer gas will be conducted. The mean air velocity and air turbulence data provided in this paper can be used for validation of CFD models which permits more comprehensive studies on the effect of multiple factors on airflow patterns both indoors and around the building.

**Author Contributions:** Conceptualization, Q.Y., B.A. and T.A.; methodology, Q.Y., D.J. and G.Z.; validation, Q.Y., D.J. and L.T.; formal analysis, Q.Y.; investigation, Q.Y. and L.T.; writing—original draft preparation, Q.Y.; writing—review and editing, D.J., L.T., G.Z., B.A., S.H., Š.N., E.H. and T.A.; supervision, G.Z. and T.A.; project administration, T.A.; funding acquisition, T.A. All authors have read and agreed to the published version of the manuscript.

**Funding:** This research was an accompanying study of the research project “Emissionsminderung Nutztierhaltung” (EmiMin FKZ) funded by German Federal Ministry of Food and Agriculture (BMEL) and the Federal Office for Agriculture and Food (BLE).

**Acknowledgments:** The authors greatly acknowledge the technicians Andreas Reinhardt and Ulrich Stollberg at ATB for the construction of the scaled model, and for their technical support in the wind tunnel experiment. We also appreciate the staff at Institute of Agricultural Process Engineering, CAU for providing all information about the prototype pig barn.

**Conflicts of Interest:** The authors declare no conflict of interest.

## References

1. Stavrakakis, G.M.; Koukou, M.K.; Vrachopoulos, M.G.; Markatos, N.C. Natural cross-ventilation in buildings: Building-scale experiments, numerical simulation and thermal comfort evaluation. *Energy Build.* **2008**, *40*, 1666–1681. [\[CrossRef\]](#)
2. De Paepe, M.D.; Pieters, J.G.; Cornelis, W.M.; Gabriels, D.; Merci, B.; Demeyer, P. Airflow measurements in and around scale model cattle barns in a wind tunnel: Effect of ventilation opening height. *Biosyst. Eng.* **2012**, *113*, 22–32. [\[CrossRef\]](#)
3. Honeyman, M.S. Extensive bedded indoor and outdoor pig production systems in USA: Current trends and effects on animal care and product quality. *Livest. Prod. Sci.* **2005**, *94*, 15–24. [\[CrossRef\]](#)
4. Park, H.-S.; Min, B.; Oh, S.-H. Research trends in outdoor pig production—A review. *Asian-Australas J. Anim. Sci.* **2017**, *30*, 1207–1214. [\[CrossRef\]](#)
5. Gade, P.B. Welfare of animal production in intensive and organic systems with special reference to Danish organic pig production. *Meat Sci.* **2002**, *62*, 353–358. [\[CrossRef\]](#)
6. Møller, F. Housing of finishing pigs within organic farming. In *Ecological Animal Husbandry in the Nordic Countries, Proceedings of the NJF-Seminar No. 303, Horsens, Denmark, 16–17 September 1999*; Danish Research Centre for Organic Farming: Horsens, Denmark, 1999; pp. 93–98.
7. Hansen, L.L.; Claudi-Magnussen, C.; Jensen, S.K.; Andersen, H.J. Effect of organic pig production systems on performance and meat quality. *Meat Sci.* **2006**, *74*, 605–615. [\[CrossRef\]](#)
8. Fraser, D. Understanding animal welfare. *Acta Vet. Scand.* **2008**, *50*, S1. [\[CrossRef\]](#)
9. Ikeguchi, A.; Zhang, G.; Okushima, L.; Bennetsen, J.C. Windward windbreak effects on airflow in and around a scale model of a naturally ventilated pig barn. *Trans. ASAE* **2003**, *46*, 789–795. [\[CrossRef\]](#)
10. Mendes, L.B.; Pieters, J.G.; Snoek, D.; Ogink, N.W.M.; Brusselman, E.; Demeyer, P. Reduction of ammonia emissions from dairy cattle cubicle houses via improved management- or design-based strategies: A modeling approach. *Sci. Total Environ.* **2017**, *574*, 520–531. [\[CrossRef\]](#)
11. Aubrun, S.; Leitl, B. Unsteady characteristics of the dispersion process in the vicinity of a pig barn. Wind tunnel experiments and comparison with field data. *Atmos. Environ.* **2004**, *38*, 81–93. [\[CrossRef\]](#)
12. Samer, M.; Ammon, C.; Loebstin, C.; Fiedler, M.; Berg, W.; Sanftleben, P.; Brunsch, R. Moisture balance and tracer gas technique for ventilation rates measurement and greenhouse gases and ammonia emissions quantification in naturally ventilated buildings. *Build. Environ.* **2012**, *50*, 10–20. [\[CrossRef\]](#)
13. Pasquill, F. *Atmospheric Diffusion: The Dispersion of Windborne Material from Industrial and Other Sources*, 2nd ed.; Ellis Horwood Ltd.: Chichester, UK, 1974.
14. Wyngaard, J.C.; Brost, R.A. Top-down and bottom-up diffusion of a scalar in the convective boundary layer. *J. Atmos. Sci.* **1984**, *41*, 102–112. [\[CrossRef\]](#)
15. Angevine, W.M.; Edwards, J.M.; Lothon, M.; LeMone, M.A.; Osborne, S.R. Transition periods in the diurnally-varying atmospheric boundary layer over land. *Bound. -Layer Meteorol.* **2020**, 1–19. [\[CrossRef\]](#)
16. Caughey, S.J.; Wyngaard, J.C.; Kaimal, J.C. Turbulence in the evolving stable boundary layer. *J. Atmos. Sci.* **1979**, *36*, 1041–1052.
17. Sastre, M.; Yagüe, C.; Román-Cascón, C.; Maqueda, G. Atmospheric boundary-layer evening transitions: A comparison between two different experimental sites. *Bound. -Layer Meteorol.* **2015**, *157*, 375–399. [\[CrossRef\]](#)
18. Ikeguchi, A.; Okushima, L. Airflow patterns related to polluted air dispersion in open free-stall dairy houses with different roof shapes. *Trans. ASAE* **2001**, *44*, 1797–1805. [\[CrossRef\]](#)
19. Tyndall, J.; Colletti, J. Mitigating swine odor with strategically designed shelterbelt systems: A review. *Agroforest. Syst.* **2007**, *69*, 45–65. [\[CrossRef\]](#)
20. Lin, X.-J.; Barrington, S.; Nicell, J.; Choiniere, D.; Vezina, A. Influence of windbreaks on livestock odour dispersion plume in the field. *Agric. Ecosyst. Environ.* **2006**, *116*, 263–272. [\[CrossRef\]](#)
21. Bottcher, R.W.; Keener, K.M.; Munilla, R.D. *Comparison of Odor Control Mechanisms for Wet Pad Scrubbing, Indoor Ozonation, Windbreak Walls and Biofilters*; ASAE Paper; ASAE: St. Joseph, MI, USA, 2000; pp. 49085–49659.
22. Parker, D.B.; Malone, G.W.; Walter, W.D. Vegetative environmental buffers and exhaust fan deflectors for reducing downwind odor and VOCs from tunnel-ventilated swine barns. *Trans. ASABE* **2012**, *55*, 227–240. [\[CrossRef\]](#)

23. Tominaga, Y.; Akabayashi, S.-I.; Kitahara, T.; Arinami, Y. Air flow around isolated gable-roof buildings with different roof pitches: Wind tunnel experiments and CFD simulations. *Build. Environ.* **2015**, *84*, 204–213. [[CrossRef](#)]
24. Yi, Q.; Li, H.; Wang, X.; Zong, C.; Zhang, G. Numerical investigation on the effects of building configuration on discharge coefficient for a cross-ventilated dairy building model. *Biosyst. Eng.* **2019**, *182*, 107–122. [[CrossRef](#)]
25. Sauer, T.; Hatfield, J.L.; Haan, F.L. A wind tunnel study of airflow near model swine confinement buildings. *Trans. ASABE* **2011**, *54*, 643–652. [[CrossRef](#)]
26. Ahmad, K.; Khare, M.; Chaudhry, K.K. Wind tunnel simulation studies on dispersion at urban street canyons and intersections—A review. *J. Wind Eng. Ind. Aerodyn.* **2005**, *93*, 697–717. [[CrossRef](#)]
27. Huang, Y.-D.; Xu, X.; Liu, Z.-Y.; Deng, J.-T.; Kim, C.-N. Impacts of shape and height of building roof on airflow and pollutant dispersion inside an isolated street canyon. *Environ. Forensics* **2016**, *17*, 361–379. [[CrossRef](#)]
28. Takano, Y.Y.; Moonen, P. On the influence of roof shape on flow and dispersion in an urban street canyon. *J. Wind Eng. Ind. Aerodyn.* **2013**, *123*, 107–120. [[CrossRef](#)]
29. Lee, I.-B.; Kang, C.; Lee, S.; Kim, G.; Heo, J.; Sase, S. Development of vertical wind and turbulence profiles of wind tunnel boundary layers. *Trans. ASAE* **2004**, *47*, 1717–1726. [[CrossRef](#)]
30. Lee, I.; Sase, S.; Okushima, L.; Ikeguchi, A.; Choi, K.; Yun, J. A wind tunnel study of natural ventilation for multi-span greenhouse scale models using two-dimensional particle image velocimetry (PIV). *Trans. ASAE* **2003**, *46*, 763–772.
31. Etheridge, D.W.; Sandberg, M. *Building Ventilation: Theory and Measurement*; John Wiley & Sons: Chichester, UK, 1996.
32. Olsen, A.W.; Dybkjær, L.; Simonsen, H.B. Behaviour of growing pigs kept in pens with outdoor runs II. Temperature regulatory behaviour, comfort behaviour and dunging preferences. *Livest. Prod. Sci.* **2001**, *69*, 265–278. [[CrossRef](#)]
33. Nosek, Š.; Kluková, Z.; Jakubcová, M.; Yi, Q.; Janke, D.; Demeyer, P.; Jaňour, Z. The impact of atmospheric boundary layer, opening configuration and presence of animals on the ventilation of a cattle barn. *J. Wind Eng. Ind. Aerodyn.* **2020**, *201*, 104185. [[CrossRef](#)]
34. Amon, T.; Yi, Q.; Heinicke, J.; Pinto, S.; Hoffmann, G.; Hempel, S.; Siemens, T.M.; Janke, D.; Ammon, C.; Amon, B. Optimisation of environment-animal-welfare interactions in high-performance dairy cows housed in naturally ventilated barns. In Proceedings of the 2019 International Symposium on Animal Environment and Welfare (2019 ISAEW), Chongqing, China, 21–24 October 2019; pp. 223–231.
35. König, M.; Bonkoš, K.; Amon, T. Wind tunnel measurements on reduction of near surface concentrations through naturally barrier on emissions from naturally ventilated barn. In Proceedings of the Physmod 2017—International Workshop on Physical Modelling of Flow and Dispersion Phenomena, Dynamics of Urban and Coastal Atmosphere, Nantes, France, 23–25 August 2017.
36. Yi, Q.; König, M.; Janke, D.; Hempel, S.; Zhang, G.; Amon, B.; Amon, T. Wind tunnel investigations of sidewall opening effects on indoor airflows of a cross-ventilated dairy building. *Energy Build.* **2018**, *175*, 163–172. [[CrossRef](#)]
37. Yi, Q.; Zhang, G.; König, M.; Janke, D.; Hempel, S.; Amon, T. Investigation of discharge coefficient for wind-driven naturally ventilated dairy barns. *Energy Build.* **2018**, *165*, 132–140. [[CrossRef](#)]
38. Yi, Q.; Wang, X.; Zhang, G.; Li, H.; Janke, D.; Amon, T. Assessing effects of wind speed and wind direction on discharge coefficient of sidewall opening in a dairy building model—A numerical study. *Comput. Electron. Agric.* **2019**, *162*, 235–245. [[CrossRef](#)]
39. Yi, Q.; Zhang, G.; Li, H.; Wang, X.; Janke, D.; Amon, B.; Hempel, S.; Amon, T. Estimation of opening discharge coefficient of naturally ventilated dairy buildings by response surface methodology. *Comput. Electron. Agric.* **2020**, *169*, 105224. [[CrossRef](#)]
40. VDI, Guideline 3783/12. In *Physical Modelling of Flow and Dispersion Processes in the Atmospheric Boundary Layer—Application of Wind Tunnels*; Beuth Verlag: Berlin, Germany, 2000; Volume 3783/12.
41. Uehara, K.; Wakamatsu, S.; Ooka, R. Studies on critical Reynolds number indices for wind-tunnel experiments on flow within urban areas. *Bound. -Layer Meteorol.* **2003**, *107*, 353–370. [[CrossRef](#)]
42. Castro, I.P.; Robins, A.R. The flow around a surface-mounted cube in uniform and turbulent streams. *J. Fluid Mech.* **1977**, *79*, 307–335. [[CrossRef](#)]

43. Snyder, W.H. Similarity criteria for the application of fluid models to the study of air pollution meteorology. *Bound. -Layer Meteorol.* **1972**, *3*, 113–134. [[CrossRef](#)]
44. Shimogata, S.; Sugawara, K.; Yokoyama, O. Wind tunnel experiment of diffusion of exhaust gas emitted from roof ventilator of long factory building. *Pollut. Control* **1974**, *9*, 62–70.
45. Ntinis, G.K.; Zhang, G.; Fragos, V.P.; Bochtis, D.D.; Nikita-Martzopoulou, C. Airflow patterns around obstacles with arched and pitched roofs: Wind tunnel measurements and direct simulation. *Eur. J. Mech. B Fluid.* **2014**, *43*, 216–229. [[CrossRef](#)]
46. Tominaga, Y.; Blocken, B. Wind tunnel experiments on cross-ventilation flow of a generic building with contaminant dispersion in unsheltered and sheltered conditions. *Build. Environ.* **2015**, *92*, 452–461. [[CrossRef](#)]



© 2020 by the authors. Licensee MDPI, Basel, Switzerland. This article is an open access article distributed under the terms and conditions of the Creative Commons Attribution (CC BY) license (<http://creativecommons.org/licenses/by/4.0/>).